Unsteady Aerodynamic Modeling of a Fighter Wing in Transonic Flow

J.B. Malone*
Lockheed-Georgia Company, Marietta, Georgia
L.N. Sankar†
Georgia Institute of Technology, Atlanta, Georgia
and
W.A. Sotomayer‡
Air Force Wright Aeronautical Laboratories, Wright-Patterson AFB, Ohio

A numerical method for predicting steady and unsteady aerodynamic flows about aircraft wing configurations is presented. The numerical procedure solves the three-dimensional full-potential equation by a strongly implicit approximate factorization algorithm. Steady-flow analyses are obtained by relaxation, while unsteady analyses are calculated by time-accurate marching. In the present work, calculated steady, quasisteady, and unsteady wing surface pressures are presented for an F-5 fighter configuration and compared to experimental data for subsonic and transonic flight conditions.

Nomenclature

a	= speed of sound
$A_1,\ldots,A_6$	= metrics of coordinate transformation
c	= reference chord
C_p	= steady-flow pressure coefficient, $=(P-P_\infty)/q_\infty$
C_p'	= unsteady-flow pressure coefficient, real part
C_p''	= unsteady-flow pressure coefficient, imaginary part
G	= reduced velocity potential, $=\phi-\phi_\infty$
$\dot{h}$	= plunging velocity
J	= Jacobian of coordinate transformation
M	= Mach number
P	= static pressure
q	= fluid velocity
t	= time
u,v,w	= components of local velocity in x,y,z directions, respectively
U,V,W	= contravariant velocity components
x,y,z	= physical coordinate system
X_N	= x coordinate of wing mode-shape node line
α_0	= freestream angle of attack
$\dot{\alpha}$	= angular velocity
$\Delta\alpha(t)$	= incremental angle-of-attack change at time t
γ	= ratio of specific heats
ξ,η,ζ	= computational coordinate system
ρ	= fluid density
τ	= time in transformed plane
ϕ	= velocity potential

Subscripts

L,U	= lower and upper surfaces of wing, respectively
LE	= quantity at leading edge of wing
max	= maximum value of indicated quantity
∞	= conditions at large distances from wing

Presented as Paper 84-1566 at the AIAA 17th Fluid Dynamics, Plasma Dynamics, and Lasers Conference, Snowmass, CO, June 25-27, 1984; received July 1, 1984; revision received Feb. 19, 1986.

*Senior Scientist, Advanced Flight Sciences Department. Member AIAA.
†Associate Professor, School of Aerospace Engineering. Member AIAA.
‡Aerospace Engineer. Member AIAA.

Introduction

MODERN fighter aircraft typically require low-aspect-ratio, highly tapered wings and can experience significant aeroelastic effects during flight. For fighters with tip-mounted stores, these effects are especially important and can result in flutter phenomena that may greatly limit the useful flight envelope. Accurate estimation of flutter phenomena is of extreme importance in the overall analysis and design of fighter aircraft configurations.

Flight at transonic Mach numbers is typically accompanied by a significant decrease in airplane flutter speed. This cannot be adequately predicted by extrapolating unsteady subsonic aerodynamic theories into the transonic flow regime. Instead, accurate transonic flutter analyses must incorporate aerodynamic methods that properly account for shock-wave development and motion.

For three-dimensional, unsteady, potential-flow problems, computer programs using time-accurate, finite-difference methods have been developed by several researchers. Borland et al.[1] have developed a procedure based on a small-disturbance formulation. Methods based on full-potential formulations have been developed by Steger and Caradonna,[2] Sankar et al.,[3] Isogai,[4] Bridgeman et al.,[5] and Shankar et al.[6]

The present paper describes a computational aerodynamics method for solutions to the three-dimensional full-potential equation. The method is an improved version of the numerical procedure described in Ref. 3 for steady and unsteady transonic flows about aircraft wing configurations. In this paper, the computational method is described and computed results are compared with experimental data for an F-5 fighter wing model.[7]

Mathematical Formulation

The strong conservation form of the full-potential equation

$$\rho_t+(\rho\phi_x)_x+(\rho\phi_y)_y+(\rho\phi_z)_z=0 \tag{1}$$

together with the energy and gas-law relationships

$$a_\infty^2 + [(\gamma-1)/2]q_\infty^2 = a^2 + [(\gamma-1)/2](2\phi_t + \phi_x^2 + \phi_y^2 + \phi_z^2) \tag{2}$$

$$\rho = \rho_\infty (a^2/a_\infty^2)^{1/(\gamma-1)} \tag{3}$$

form the basis of the finite-difference algorithm.

For the sake of convenience, all densities are nondimensionalized with respect to ρ_∞ and all velocities with respect to V_∞. The length scales are nondimensionalized with respect to c, and the time quantities are nondimensionalized with respect to c/q.

The above equations may be readily recast in a strong conservation form in a coordinate system (ξ,η,ζ,τ), which is related to the physical coordinates (x,y,z,t) by the following general transformation:

$$\xi = \xi(x,y,z,t),\ \eta = \eta(x,y,z,t),\ \zeta = \zeta(x,y,z,t),\ \tau = t$$

In this new coordinate system, the equation governing the conservation of mass is given by

$$(\rho/J)_\tau + (\rho U/J)_\xi + (\rho V/J)_\eta + (\rho W/J)_\zeta = 0 \tag{4}$$

where

$$J = \xi_x(\eta_y\zeta_z - \eta_z\zeta_y) + \xi_y(\eta_z\zeta_x - \eta_x\zeta_z) + \xi_z(\eta_x\zeta_y - \eta_y\zeta_x) \tag{5}$$

The conservation of energy equation, when coupled with the isentropic gas relationship, is given by

$$\rho = 1 + [(\gamma-1)/2] \times M_\infty^2 [1 - 2\phi_\tau - (U+\xi_t)\phi_\xi - (V+\eta_t)\phi_\eta - (W+\zeta_t)\phi_\zeta]^{1/(\gamma-1)} \tag{6}$$

In Eqs. (4) and (6), the kinematic and geometric quantities are defined by the following equations.

Coordinate velocities:

$$\begin{Bmatrix} \xi_t \\ \eta_t \\ \zeta_t \end{Bmatrix} = -\left[\begin{Bmatrix} \xi_x \\ \eta_x \\ \zeta_x \end{Bmatrix} x_\tau + \begin{Bmatrix} \xi_y \\ \eta_y \\ \zeta_y \end{Bmatrix} y_\tau + \begin{Bmatrix} \xi_z \\ \eta_z \\ \zeta_z \end{Bmatrix} z_\tau \right] \tag{7}$$

Contravariant velocities:

$$\begin{Bmatrix} U \\ V \\ W \end{Bmatrix} = \begin{Bmatrix} \xi_t \\ \eta_t \\ \zeta_t \end{Bmatrix} + \begin{Bmatrix} A_1 \\ A_2 \\ A_3 \end{Bmatrix} \phi_\xi + \begin{Bmatrix} A_2 \\ A_4 \\ A_5 \end{Bmatrix} \phi_\eta + \begin{Bmatrix} A_3 \\ A_5 \\ A_6 \end{Bmatrix} \phi_\zeta \tag{8}$$

Metric quantities:

$$\begin{bmatrix} A_1A_2A_3 \\ A_2A_4A_5 \\ A_3A_5A_6 \end{bmatrix} = \begin{bmatrix} \xi_x\ \xi_y\ \xi_z \\ \eta_x\ \eta_y\ \eta_z \\ \zeta_x\ \zeta_y\ \zeta_z \end{bmatrix} \begin{bmatrix} \xi_x\ \eta_x\ \zeta_x \\ \xi_y\ \eta_y\ \zeta_y \\ \xi_z\ \eta_z\ \zeta_z \end{bmatrix} \tag{9}$$

In Eq. (5), the term $(\rho/J)_\tau$ is replaced by a new expression using a straightforward differentiation of Eq. (6) with respect to τ. After performing the above differentiation, the following equation is obtained in place of Eq. (5):

$$(\rho^{2-\gamma}/J)M_\infty^2[\phi_{\tau\tau} + U\phi_{\xi\tau} + V\phi_{\eta\tau} + W\phi_{\zeta\tau}] + Q_1 = (\rho U/J)_\xi + (\rho V/J)_\eta + (\rho W/J)_\zeta \tag{10}$$

where

$$Q_1 = -\rho(1/J)_\tau + (\rho^{2-\gamma}/2J)M_\infty^2[A_{1\tau}\phi_\xi^2 + A_{4\tau}\phi_\eta^2 + A_{6\tau}\phi_\zeta^2] + \phi_\xi\phi_\eta A_{2\tau} + \phi_\eta\phi_\zeta A_{5\tau} + \phi_\xi\phi_\zeta A_{3\tau} + \phi_\xi(\xi_t)_\tau + \phi_\eta(\eta_t)_\tau + \phi_\eta(\zeta_t)_\tau \tag{11}$$

The Q_1 term derives its contribution entirely from the time deformation of the grid. For problems where the grid undergoes only small deformations, Q_1 may be explicitly evaluated without any instability. For problems involving large deformations, Q_1 must be implicitly treated and linearized at time level $(n+1)$. An implicit treatment of the contributions from grid deformation is given in Malone and Sankar.[8]

Equation (11) is highly nonlinear, as well as nonconservative with respect to time. Ballhaus and Steger[9] have demonstrated that a nonconservative treatment (with respect to time) of the unsteady potential equation can give erroneous shock speeds in transonic flows. Thus, Eq. (10) in its present form is useful only for subsonic flows.

A strict conservation form in time may be obtained as follows. Let $L^{n+1}(\phi)$ represent the left-hand side of Eq. (10) at the time level $(n+1)$.

Then, in order to exactly balance the terms in $L^{n+1}(\phi)$, the following quantity

$$L^n(\phi) + \frac{1}{\Delta t}\left[\left(\frac{\rho}{J}\right)^n - \left(\frac{\rho}{J}\right)^{n-1}\right] \approx 0 \tag{12}$$

is added to the right-hand side of the equation. Thus Eq. (10) becomes

$$L^{n+1}(\phi) = L^n(\phi) + \frac{1}{\Delta t}\left[\left(\frac{\rho}{J}\right)^n - \left(\frac{\rho}{J}\right)^{n-1}\right] + \left(\frac{\rho U}{J}\right)_\xi^{n+1} + \left(\frac{\rho V}{J}\right)_\eta^{n+1} + \left(\frac{\rho W}{J}\right)_\zeta^{n+1} \tag{13}$$

This equation can be placed in a conservative divergence form in both the time and space coordinates. The above equation is nonlinear in time, and must be linearized. In order to maintain strict conservation with respect to time, both $L^{n+1}(\phi)$ and $L^n(\phi)$ are linearized in an identical manner. It may be noted that Eq. (13) still contains ρ. Thus Eq. (7) must still be used, albeit in an auxiliary role, during the computation.

Experience with full-potential solution procedures[10] has shown that it is advantageous to recast Eqs. (13) and (6) into a "reduced-potential" form. Here, the reduced potential is defined as the difference between the actual velocity potential and the uniform freestream potential. The reduced potential is given by the following equation:

$$G = \phi - \phi_\infty \tag{14}$$

and

$$\phi_\infty = x\cos\alpha + z\sin\alpha \tag{15}$$

When Eq. (14) is substituted into Eq. (13), terms involving derivatives ξ and ζ of the total potential ϕ can be written as

$$\phi_\xi = G_\xi + x_\xi \cos\alpha + z_\xi \sin\alpha \tag{16}$$

and

$$\phi_\zeta = G_\zeta + x_\zeta \cos\alpha + z_\zeta \sin\alpha \tag{17}$$

Equation (13) is then rewritten for solution in terms of the reduced-potential as follows:

$$L^{n+1}(G) = L^n(G) + \frac{1}{\Delta t}\left[\left(\frac{\rho}{J}\right)^n - \left(\frac{\rho}{J}\right)^{n-1}\right] + \left(\frac{\rho U}{J}\right)_\xi^{n+1} + \left(\frac{\rho V}{J}\right)_\eta^{n+1} + \left(\frac{\rho W}{J}\right)_\zeta^{n+1} \tag{18}$$

From Eqs. (16) and (17), it is seen that the use of a reduced-potential formulation permits the analytical evaluation of certain portions of the partial derivatives required for Eq. (18), thus reducing numerical errors, even on highly distorted or stretched computation grids.[2]

Computation Grid

The well-known parabolic coordinate transformation[11] is used to construct a body-fitted coordinate system suitable for modeling aerodynamic flows around wall-mounted swept wings. In this coordinate system the wing surface, as well as any assumed wake shape, becomes a coordinate surface such as $\zeta = 0$. The outer boundary in the direction normal to the wing surface is located at $\zeta = \zeta_{\max}$. The sidewalls are mapped onto the plane $\eta = 0$. The wingtip is located at $\eta = \eta_{\text{tip}}$, while the outer boundary in the wing spanwise direction is located at $\eta = \eta_{\max}$. Finally, the streamwise coordinate ξ is defined as $\xi = 1$ at the downstream boundary, lower wake position, and as $\xi = \xi_{\max}$ at the downstream boundary, upper-wake location. The wing leading edge is located at

$$\xi_{\text{LE}} = (\xi_{\max} + 1)/2 \tag{19}$$

Figures 1 and 2 illustrate this numerical grid in both physical and computational space.

Continuation of the sheared parabolic transformation beyond the wingtip introduces a singular line requiring special treatment. In the present work, the wing is extended beyond its tip with fluid airfoils of very small but finite thickness. Since these are fluid airfoils, ϕ must be continuous across them, and appropriate action is taken while applying the boundary conditions on the fluid airfoil surface.

In the computational domain the grid points are uniformly placed so that $\Delta\xi = \Delta\eta = \Delta\zeta = 1$. In the physical plane (x,y,z), the grid points are clustered closely near the wing and are highly stretched in the outer regions.

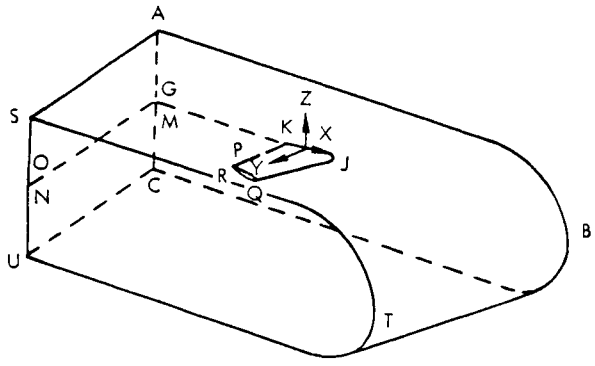

Fig. 1 C-grid coordinate system—physical space.

Boundary Conditions

The boundary conditions used approximate the flow about a finite wing which is mounted on a wall (symmetry plane) located at the wing root. The necessary boundary conditions can be divided into the following regions.

Wing Surface

For inviscid flows, the condition of zero normal velocity at the wing surface is satisfied by setting

$$W = 0 \tag{20}$$

This equation is used to obtain an expression for the derivative of G on the wing surface. That is,

$$G_\zeta = -\frac{1}{A_6}[\zeta_t + \zeta_x(G_\xi \xi_x + G_\eta \eta_x + \cos\alpha) + \zeta_y(G_\xi \xi_y + G_\eta \eta_y) + \zeta_z(G_\xi \xi_z + G_\eta \eta_z + \sin\alpha)] \tag{21}$$

Wake Surface

At the vortex sheet (located on the wing mean plane) the requirement that the pressure and W be continuous leads to the following transport equation for shed vorticity:

$$\frac{\partial \Gamma}{\partial t} + u\frac{\partial \Gamma}{\partial x} = 0 \tag{22}$$

Here u is the average of the x component of velocities above and below the vortex sheet and Γ is the jump in the velocity potential. The above equation is integrated using an explicit marching procedure in x, starting from the wing trailing edge at each span station. Once Γ is determined, the values G_U and G_L above and below the vortex sheet are obtained using the following relations:

$$\Gamma = G_U - G_L \tag{23}$$

$$(G_z)_U - (G_z)_L \tag{24}$$

Wingtip Extension

At points beyond the wingtip, infinitesimally thin airfoil sections are assumed to avoid treating a special equation near points on the singular axis. No discontinuity in G is permitted across these fluid airfoils. On the fluid airfoil section, everywhere except at the nose, there are two computational points: one on the upper surface and the other on the lower surface of the airfoil. The values of G on these airfoil stations are determined by a simple averaging of G above and

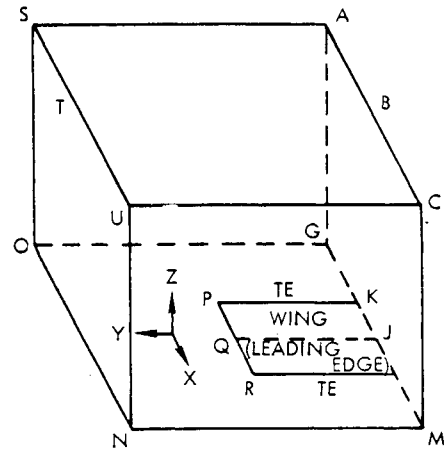

Fig. 2 C-grid coordinate system—computational space.

below. At the nose of the fluid airfoil, where such averaging is not possible, the Laplace equation is solved for G, as suggested by Jameson.[10]

Symmetry Plane

At the end wall, the governing equation is applied. The proper boundary condition at the end wall is that the contravariant velocity V becomes zero. This was satisfied by creating image points behind the wall and setting

$$(\rho V/J)_{i,j-1/2,k} = -(\rho V/J)_{i,j+1/2,k} \tag{25}$$

Outer Boundaries

At the far-field boundaries, the disturbances in ϕ are assumed to vanish, both for steady- and unsteady-flow problems. Under this assumption the reduced potential vanishes along the outer boundaries. This approximation produces good numerical results for unsteady flows as long as no solution contamination occurs from reflected waves at the boundaries. The grid stretching used in the current numerical procedure has proven adequate in suppressing possible wave reflections. A more rigorous treatment of the unsteady outer boundary can be made by enforcing $\rho(t)=1$, and using the resulting expression obtained from Eq. (6) as an extrapolation formula to update the potential at the outer boundary.

Matrix Solution Procedure

Equation Linearization and Discretization

Equation (18) is a nonlinear expression due to products of the reduced potential and its derivatives at the same time or iteration level. However, a first-order-accurate expression in time for $L^{n+1}(G)$ may be obtained by lagging the contravariant velocity terms. L^{n+1} is then written as

$$L^{n+1}(G) = (\rho/J)^{2-\gamma} M_\infty^2 \times [G_{\tau\tau}^{n+1} + U^n G_{\xi\tau}^{n+1} + V^n G_{\eta\tau}^{n+1} + W^n G_{\zeta\tau}^{n+1} + Q_1] \tag{26}$$

In the present numerical procedure Q_1 is set to zero. During unsteady analyses, grid velocities x_t and z_t are computed at the wing surface and applied as surface transpiration boundary conditions. These approximations have been shown to produce good numerical results for wing motions of limited amplitude.[3]

The various terms that constitute Eq. (19) are discretized as follows. The term $G_{\tau\tau}^{n+1}$ is replaced by

$$\overleftarrow{\delta}_\tau \overleftarrow{\delta}_\tau G^{n+1} = (\Delta G^{n+1} - \Delta G^n)\Delta t^2 \tag{27}$$

where the "correction" to the velocity potential at the $n+1$ time level is

$$\Delta G^{n+1} = G^{n+1} - G^n$$

A windward finite-difference expression for the term $U^n G_{\xi\tau}^{n+1}$ is written at a point (i,j,k) as

$$U_{i,j,k}^n \overleftarrow{\delta}_\xi \overleftarrow{\delta}_\tau G_{i,j,k}^{n+1} = U_{i,j,k}^n \frac{(\Delta G_{i,j,k}^{n+1} - \Delta G_{i-1,j,k}^{n+1})}{\Delta t} \tag{28}$$

Equation (28) is suitable only when $U_{i,j,k}$ is positive. In regions where $U_{i,j,k}$ is negative, a suitable expression is $U_{i,j,k}^n(\Delta G_{i+1,j,k}^{n+1} - \Delta G_{i,j,k}^{n+1})/\Delta t$. Similar expressions apply for the terms $V^n G_{\eta\tau}^{n+1}$ and $W^n G_{\zeta\tau}^{n+1}$.

In supersonic regions, an upwind bias must be added to the transonic potential equation. In the present work this upwind bias was implemented using the artificial compressibility concept studied by Holst and Ballhaus,[12] and previously applied to two-dimensional, unsteady, potential flows by Goorjian.[13] The three flux terms on the right-hand side of Eq. (18) are replaced by the following expression:

$$\left(\frac{\hat{\rho}U}{J}\right)_\xi^{n+1} + \left(\frac{\tilde{\rho}V}{J}\right)_\eta^{n+1} + \left(\frac{\bar{\rho}W}{J}\right)_\zeta^{n+1} \tag{29}$$

where

$$\hat{\rho}_{i,j,k} = \rho_{i,j,k} + \nu_{i,j,k}\overleftarrow{\delta}_\xi \rho_{i,j,k} \tag{30a}$$

$$\tilde{\rho}_{i,j,k} = \rho_{i,j,k} + \nu_{i,j,k}\overleftarrow{\delta}_\eta \rho_{i,j,k} \tag{30b}$$

$$\bar{\rho}_{i,j,k} = \rho_{i,j,k} + \nu_{i,j,k}\overleftarrow{\delta}_\zeta \rho_{i,j,k} \tag{30c}$$

and

$$\nu = \max[0, 1 - (M_c^2/M_{i,j,k}^2)] \tag{30d}$$

Here M_c is a cutoff Mach number[12] set between 1.0 and 0.95, while $M_{i,j,k}$ is the local Mach number.

In Eq. (29) the $\hat{\rho}U/J$ flux term is linearized by lagging the cross derivative and density terms. That is,

$$(\hat{\rho}U/J)^{n+1} = \hat{\rho}^n[(A_1/J)G_\xi^{n+1} + (A_2/J)G_\eta^n + (A_3/J)G_\zeta^n] + \hat{\rho}^n[(A_1/J)(x_\xi\cos\alpha + z_\xi\sin\alpha) + (A_3/J)(x_\zeta\cos\alpha + z_\zeta\sin\alpha)] + \hat{\rho}^n[\xi_t/J]^{n+1} \tag{31}$$

Here, since Q_1 has been set to zero, the metric terms A_1, A_2, A_3, etc., do not change with time. Consequently, the superscripts on these terms have been eliminated from Eq. (31). Similar expressions are written for the V and W flux components.

It should be noted that if the computational grid does not move during unsteady calculations, Eq. (18) can be rearranged into a form similar to that used in two dimensions by Goorjian.[13] That method was based on a first-order-accurate Taylor series expansion of the fluid density. However, as shown in Ref. 3, the present approach is derived solely from the addition of certain terms to Eq. (10) to restore time accuracy. The total effect of these added terms sums to zero so that the equality of Eq. (18) is preserved. The present technique will, in fact, produce different results from the method of Ref. 13 if a moving computational grid is utilized.

All of the spatial derivatives in Eq. (29) are discretized using central differences about the grid half-points in the i, j, and k directions. Cross-derivative terms, such as $\overleftarrow{\delta}_\xi[(\rho A_2/J)G_\eta^n]$ in Eq. (31), are treated by taking averages of the appropriate second-order derivatives at grid points on either side of the given half-point location.

For steady-flow problems, Eq. (19) reduces to the following familiar form:

$$(\hat{\rho}U/J)_\xi + (\tilde{\rho}V/J)_\eta + (\bar{\rho}W/J)_\zeta = 0 \tag{32}$$

The linearization and discretization of the above equation is then carried out exactly in the same manner as for the time-dependent case. The superscripts $(n+1)$ and n are interpreted to be successive iteration levels for the steady-flow case.

Approximate Factorization Procedure

Once a body-fitted coordinate system is constructed, the governing equation in its discrete, time-linearized form may be applied at all of the interior points. In the present work, points on the symmetry plane are also treated as interior points, while points on the wing surface, as well as points on any assumed wake shape, are treated as boundary points. At each interior point, the discretized equation may be formally

written as

$$Z_{i,j,k}\Delta G^{n+1}_{i,j,k-1} + B_{i,j,k}\Delta G^{n+1}_{i,j-1,k} + D_{i,j,k}\Delta G^{n+1}_{i-1,j,k} + E_{i,j,k}\Delta G^{n+1}_{i,j,k} + F_{i,j,k}\Delta G^{n+1}_{i+1,j,k} + H_{i,j,k}\Delta G^{n+1}_{i,j+1,k} + S_{i,j,k}\Delta G^{n+1}_{i,j,k+1} = R^n \quad (33)$$

Here, ΔG^{n+1} at all boundary points is either set to zero or expressed in terms of ΔG^{n+1} at the interior points in a manner described in the section on boundary conditions. Thus, Eq. (33) may be assumed to contain only ΔG^{n+1} values at the interior points.

Equation (33) represents a system of simultaneous equations for the quantity ΔG^{n+1} at all interior points. This system may be written formally as

$$[M]\{\Delta G\}^{n+1} = \{R\}^n \quad (34)$$

A direct inversion of $[M]$, or even an iterative solution of $[M]$ by a Gauss-Seidel solution procedure, for example, is not practiced because $[M]$ usually is a very large matrix, despite its sparseness. One, therefore, usually approximates the above matrix equation by another matrix equation:

$$[M']\{\Delta G\}^{n+1} = \{R\}^n \quad (35)$$

where $[M']$ is a matrix that is easily inverted, and is similar to $[M]$.

In the present work the strongly implicit procedure, as proposed by Stone,[14] is used to replace the original matrix $[M]$ by the new matrix $[M']$. This is accomplished by adding error terms to the left-hand side of Eq. (33). A complete description of the coefficient terms in Eq. (33) and the error terms added to the original matrix, $[M]$, is given in Ref. 3.

Using Stone's approximate factorization procedure, Eq. (35) can be expressed as an LU decomposition of the new matrix, $[M']$. That is,

$$[M']\{\Delta G\}^{n+1} = [L][U]\{\Delta G\}^{n+1} = \{R\}^n \quad (36)$$

where $[L]$ and $[U]$ are lower triangular and upper triangular matrices, respectively. Equation (36) is solved for the value of G at the next time level for unsteady flows, or at the next iteration level for steady flows.

Stone's approximate factorization procedure can be used to provide a unified steady/unsteady aerodynamic analysis procedure. For steady-flow problems, the coefficients of Eq. (33) contain only contributions from the steady form of the mass conservation equation. For unsteady analyses, the appropriate time derivative contributions are added to the coefficients in Eq. (33). Then, regardless of the particular application, Stone's method is applied in an identical manner to obtain a new estimate of the reduced potential, G, at the next time or iteration level. The use of Stone's method for this type of unified aerodynamics procedure permits the development of an extremely compact computer program which is relatively easy to maintain.

Results and Discussion

The F-5 model wing-tunnel tests[7] performed by the National Aerospace Laboratory (NLR) provide an excellent aerodynamic data base for computer code evaluation purposes. During these tests wing surface-pressure distributions were measured for both steady- and unsteady-flow conditions. The F-5 clean-wing test results are used here to provide correlations with the present three-dimensional full-potential aerodynamics code. The large leading-edge sweep angle and the relatively small wing aspect ratio make the aerodynamic modeling of this configuration reasonably challenging for state-of-the-art finite-difference computational methods.[15,16]

F-5 Model Description

The F-5 wing planform has a leading-edge sweep angle of approximately 32 deg. The wing airfoil is a modified NACA 65-A-004.8 section, characterized by a droop nose extending from the airfoil leading edge to approximately the 40% chord location. Aft of the 40% chord position, the airfoil is symmetrical. The zero-angle-of-attack reference line coincides with the plane of symmetry of the rear portion of the airfoil.

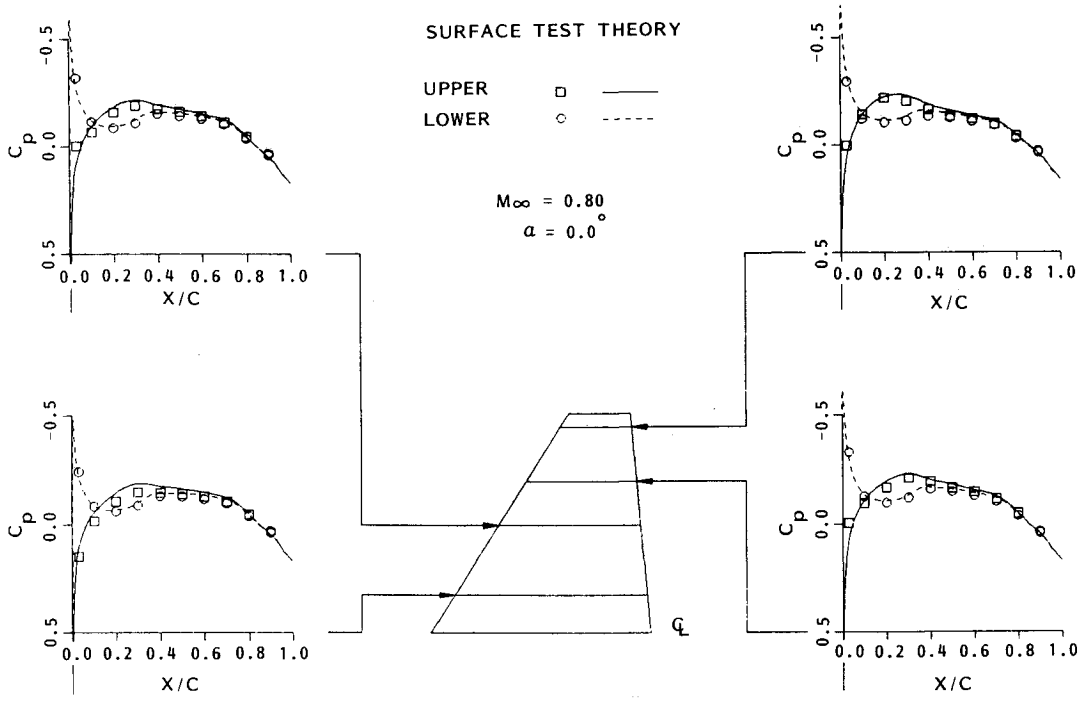

Fig. 3 F-5 steady-flow pressures, $M_\infty = 0.80$.

Aeroelastic Mode Shape

During unsteady oscillations of the F-5 model, the wing vibration mode was measured using eight accelerometers embedded in the model structure. The accelerometer data were then used to develop an analytical approximation of the wing's aeroelastic mode shape corresponding to each test condition. This analytical expression assumes no deformation in the chordwise direction and a parabolic deformation in the spanwise direction.[7] The aeroelastic mode shapes corresponding to specific test conditions were used to compute wing surface boundary conditions required for the present unsteady aerodynamic analyses.

Surface boundary conditions in the numerical computation were the velocity components in the normal and axial directions at each wing surface grid point. Velocity components at each time step were computed from the following expressions:

$$x_T = z(t)\dot{\alpha}(t) \tag{37}$$

$$z_T = -[x(t) - x_N]\dot{\alpha}(t) + \dot{h} - h_\alpha(t) \tag{38}$$

where

$$h_\alpha(t) = \tan\Delta\alpha(t) \tag{39}$$

This latter term simulates the change in wing surface slope due to unsteady incremental angle-of-attack changes.

Data Presentation

Quasisteady pressure distributions were evaluated by first computing steady-flow aerodynamic data at two incremental angles of attack above and below the mean angle ($\alpha_0 = 0$ deg), and then substituting these results into the following equation:

$$C_{pq} = \frac{\Delta C_p}{\Delta\alpha} = \frac{C_p(\alpha_0 + \Delta\alpha_1) - C_p(\alpha_0 - \Delta\alpha_1)}{2\Delta\alpha_1} \tag{40}$$

where $\alpha_1 = 0.5$ deg.

Approximations to the first harmonic components of the unsteady pressures were computed using the following expressions:

$$C_p' \cong -\left[\frac{C_{p(\omega t = 3\pi/2)} - C_{p(\omega t = \pi/2)}}{2\Delta\alpha}\right] \tag{41}$$

$$C_p'' \cong -\left[\frac{C_{p(\omega t = \pi)} - C_{p(\omega t = 0)}}{2\Delta\alpha}\right] \tag{42}$$

These expressions are exact when the pressure coefficient varies simply harmonically. Near moving shock waves, some error is possible depending upon the actual pressure variation as a function of time. A similar technique was used to estimate the first harmonic of the unsteady lift and moment coefficients.

F-5 Model Theory/Test Correlations

Numerical computations were made at Mach numbers of 0.6, 0.8, 0.9, and 0.95. For each of these Mach numbers, steady-flow analyses were made at three different angles of attack ($\alpha_0 = -0.5$, 0.0, and 0.5 deg). Then, numerical results for the 0-deg angle-of-attack cases were used as starting solutions for two unsteady-flow analyses at each of the four Mach numbers. The unsteady analyses corresponded to wing pitching oscillation frequencies of 20 and 40 Hz, respectively. Finally, quasisteady results were calculated using steady-flow analyses at $\alpha_0 = -0.5$ and $+0.5$ deg. A complete set of these theory/test data correlations can be found in Ref. 17. Several of the surface-pressure data correlations are presented here and discussed in the following paragraphs.

Steady-Flow Results

Correlations of theory and test data for steady-flow conditions are shown in Figs. 3 and 4 for $\alpha_0 = 0.0$ deg at Mach numbers of 0.8 and 0.95, respectively. In general, the correlation between test results and theory was favorable over the entire range of Mach numbers examined. At $M = 0.8$ the flow remained subcritical, which is borne out both by theoretical calculations and test data. Both test results and theory showed strong shocks at $M = 0.95$. At $M = 0.95$, test results showed shocks on both the upper and lower wing surface with the upper shock slightly aft of the lower shock.

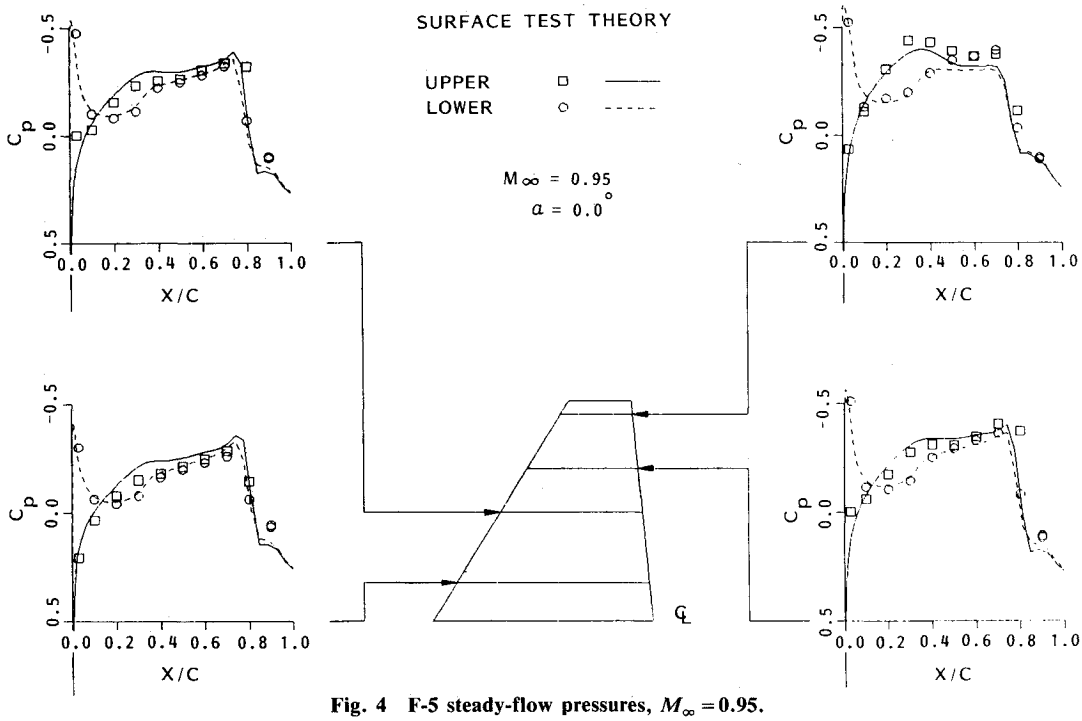

Fig. 4 F-5 steady-flow pressures, $M_\infty = 0.95$.

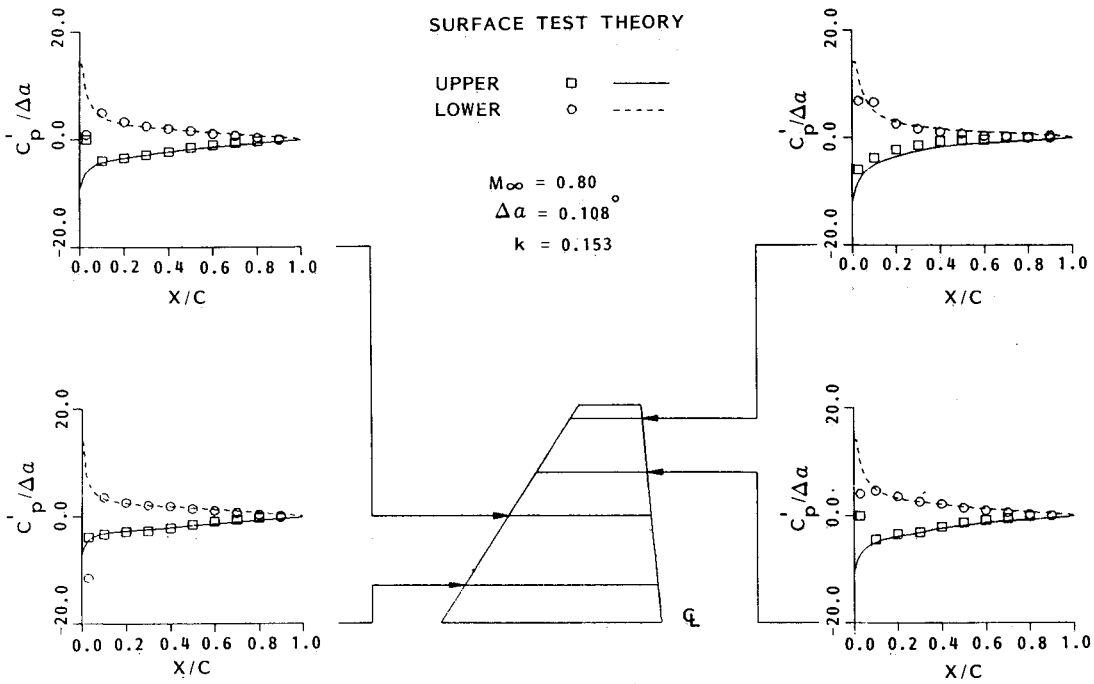

Fig. 5 Unsteady pressures, real part, $M_\infty = 0.80$.

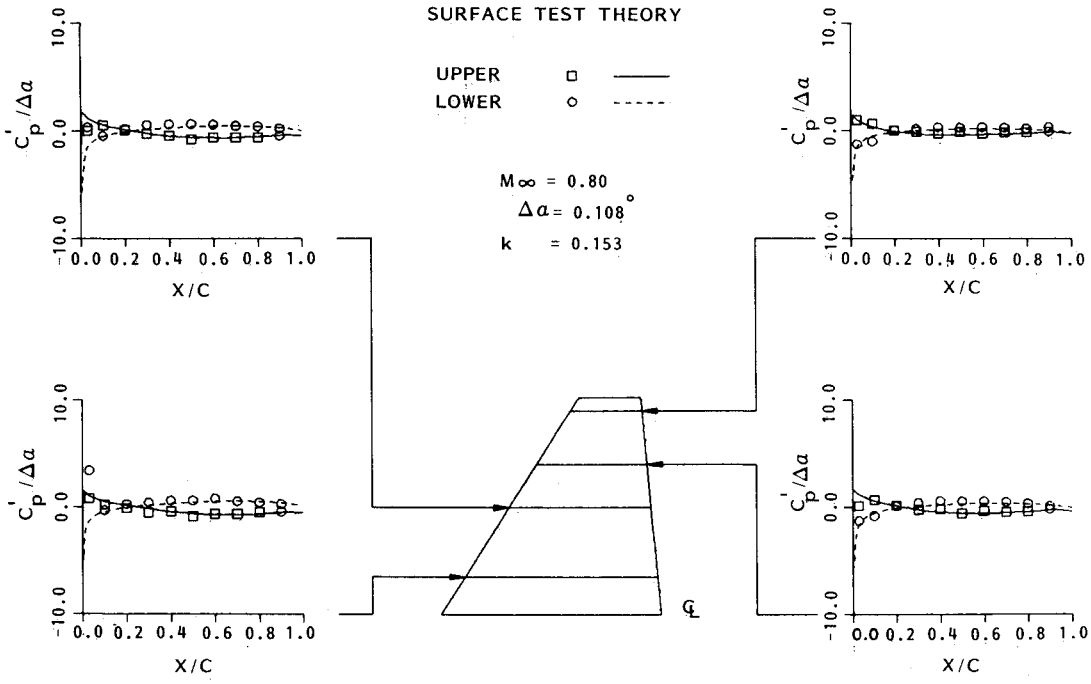

Fig. 6 Unsteady pressures, imaginary part, $M_\infty = 0.80$.

Numerical computations captured the shocks on the upper and lower wing surfaces and also placed the shock on the upper surface slightly aft.

Unsteady-Flow Results

Unsteady analysis results are shown in Figs. 5-8 for Mach numbers of 0.8 and 0.95, respectively. Estimates of the first harmonic, real and imaginary components of the unsteady surface pressures were calculated using Eqs. (41) and (42).

Each theory vs test correlation shown corresponds to a 20-Hz oscillation frequency. The reduced frequencies are nearly equal for both cases (0.130 and 0.153). The amplitude of oscillation at the wing root was 0.108 deg at Mach = 0.8 and 0.523 deg at Mach = 0.95. In calculating the results shown in these figures, each cycle of unsteady motion was divided into 240 time steps. The actual time-step size used was a function of reduced frequency. For the analyses presented here, time-step sizes ranged from 0.03 to 0.06 unit chord traveled per time step.

The real components of the lower surface pressure show a pressure peak near the leading edge caused by the drooped leading-edge wing geometry. The imaginary components of pressure are seen to be generally smaller in magnitude than the real components, except near the moving shock waves for the $M = 0.95$ case. The sign changes of the imaginary pressures on both the upper and lower surfaces are also predicted qualitatively by the theory for the $M = 0.80$ cases.

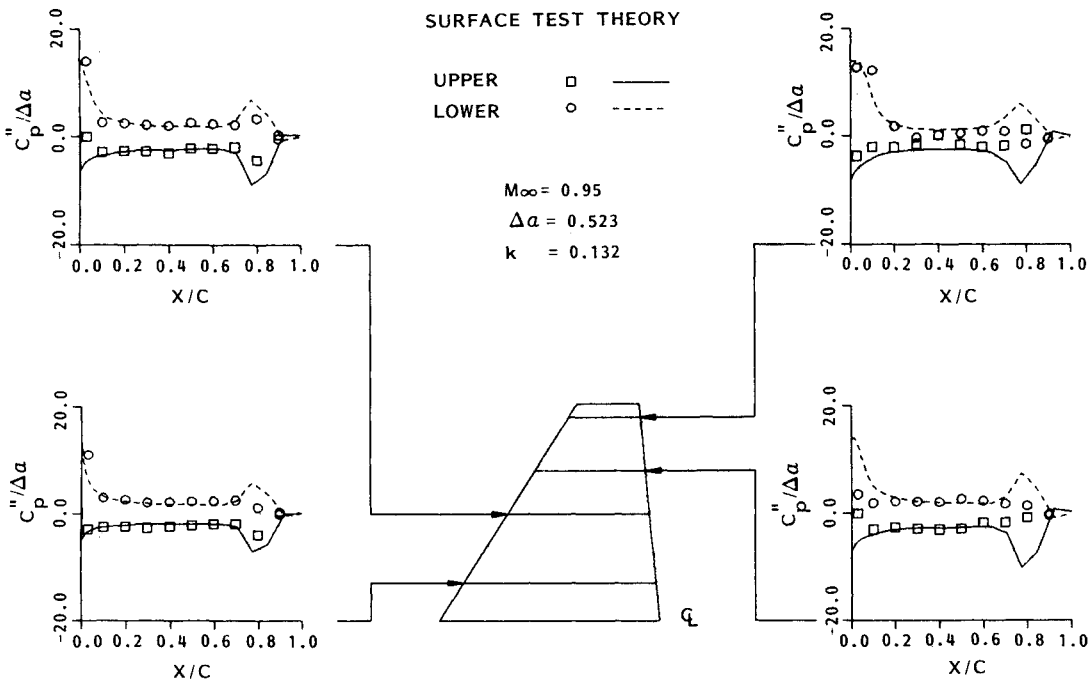

Fig. 7 Unsteady pressures, real part, $M_\infty = 0.95$.

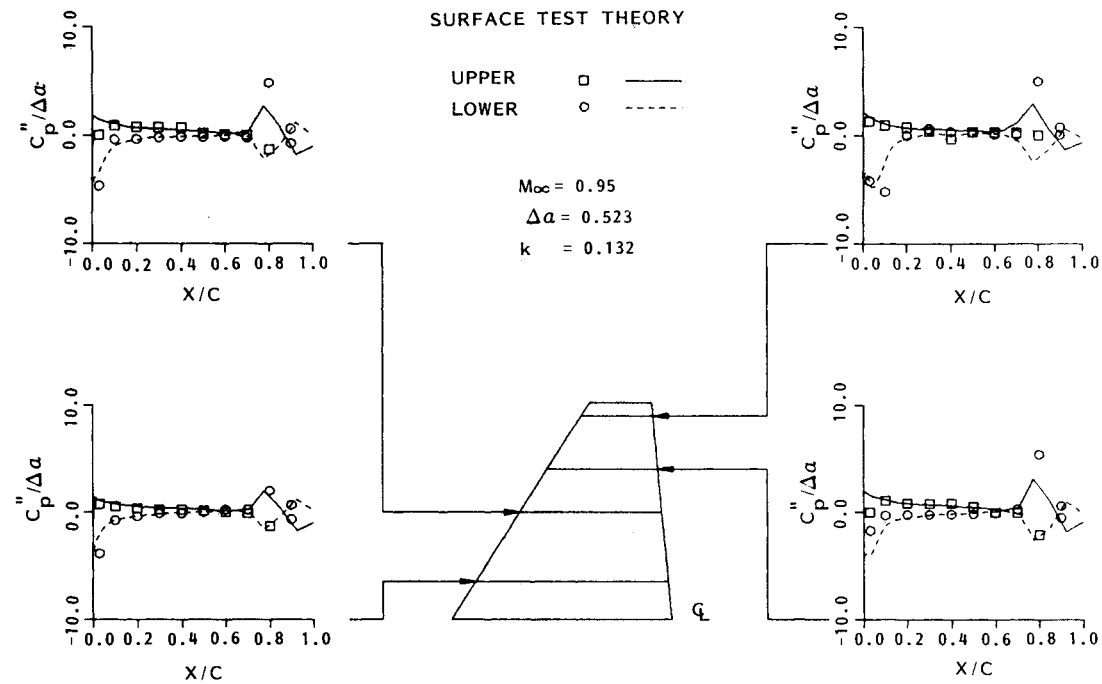

Fig. 8 Unsteady pressures, imaginary part, $M_\infty = 0.95$.

Quasisteady Results

Figures 9 and 10 show correlations of quasisteady theory and experimental data for Mach numbers of 0.80 and 0.95, respectively. The theoretical and experimental data shown in these figures were calculated using Eq. (40). Pressure data corresponding to $\alpha_0 = +0.5$ and -0.5 deg were used in the calculations. A comparison of Figs. 5 and 9 and Figs. 6 and 10 shows that the quasisteady data provide a reasonable estimate of the real component of the unsteady pressure distribution for corresponding Mach number conditions.

Concluding Remarks

A numerical algorithm for steady and unsteady potential flow was applied in the calculation of aerodynamic presures and forces on an F-5 fighter wing model in transonic flow. Correlations of calculated results and experimental data were made for steady-, quasisteady-, and unsteady-flow conditions at two values of freestream Mach number and nearly equal values of reduced frequency. These correlations showed, in general, good agreement between theory and test data for most of the cases examined. Based on these comparisons,

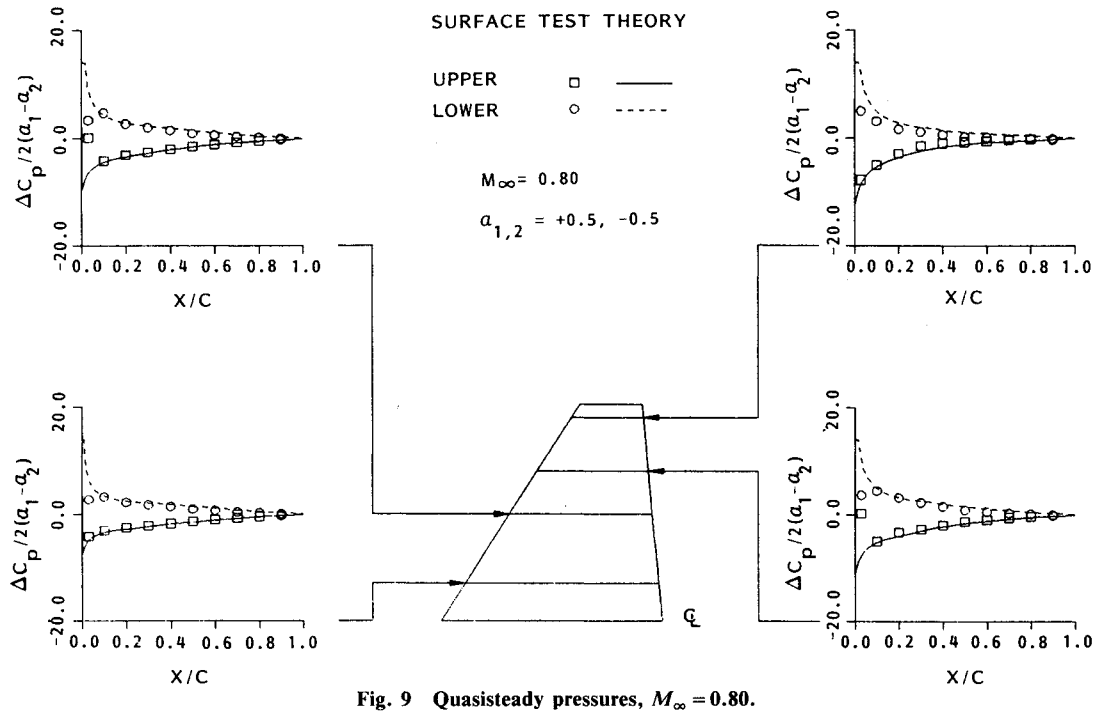

Fig. 9 Quasisteady pressures, $M_\infty = 0.80$.

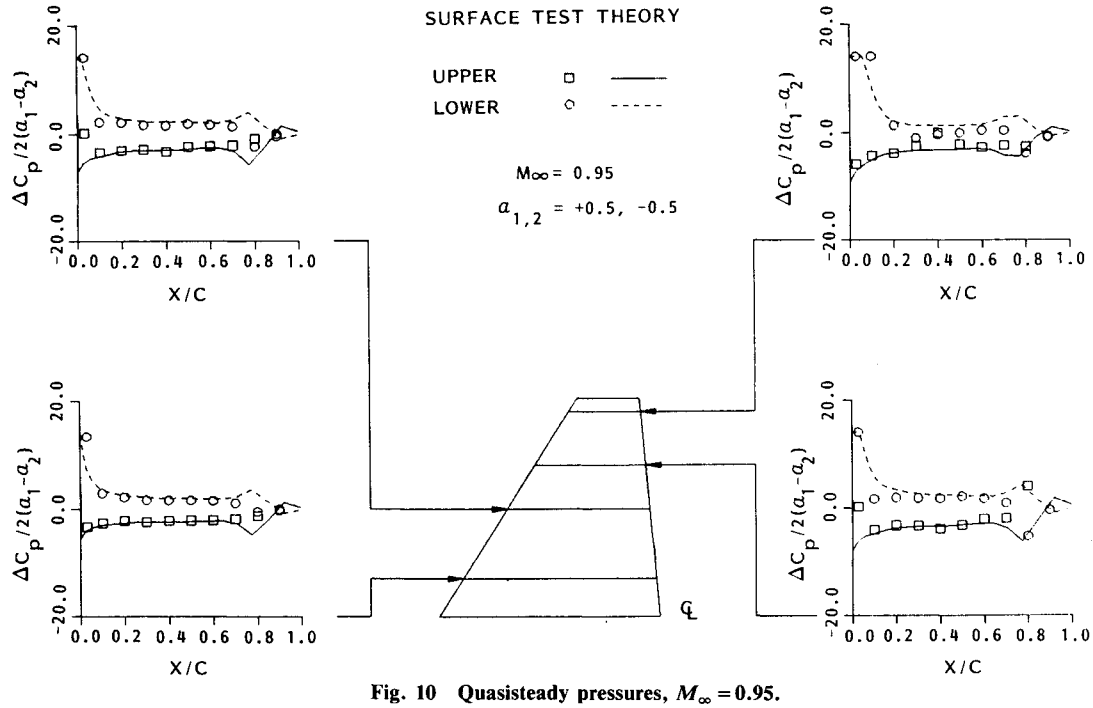

Fig. 10 Quasisteady pressures, $M_\infty = 0.95$.

a method such as the one presented herein could be used to provide the unsteady aerodynamic data required to predict the flutter behavior of fighter-type wings moving at transonic speeds.

Acknowledgments

The potential flow analysis method described in this paper was developed under Lockheed-Georgia Company's Independent Research and Development Program. The F-5 aerodynamic analyses and theory/test data correlations were sponsored by the Air Force Wright Aeronautical Laboratories under Contract F33615-83-C-3215.

References

[1]Borland, C., Rizzetta, D., and Yoshihara, H., "Numerical Solution of Three-Dimensional Unsteady Transonic Flow Over Swept Wings," AIAA Paper 80-1369, July 1980.

[2]Steger, J.L. and Caradonna, F.X., "A Conservative Implicit Finite Difference Algorithm for the Unsteady Transonic Full Potential Equation," AIAA Paper 80-1368, 1980.

[3]Sankar, L.N., Malone, J.B., and Tassa, Y., "An Implicit Conservative Algorithm for Steady and Unsteady Three-Dimensional Transonic Potential Flows," *Proceedings of the AIAA Fifth Computational Fluid Dynamics Conference*, Palo Alto, CA, June 1981, pp. 199-212.

[4]Isogai, K., "Calculation of Unsteady Transonic Potential Flow Over Oscillating Three-Dimensional Wings," NAL TR-706T, March 1982.

[5]Bridgman, J.S., Steger, J.L., and Caradonna, F.X., "A Conservative Finite Difference Algorithm for the Unsteady Transonic Potential Equation in Generalized Coordinates," AIAA Paper 82-1388, Aug. 1982.

[6]Shankar, V., Ide, H., Gorski, J., and Osher, S., "A Fast, Time-Accurate Unsteady Full Potential Scheme," *Proceedings of the AIAA 7th Computational Fluid Dynamics Conference*, Cincinnati, OH, July 1985, pp. 214-227.

[7]Tijdeman, H. et al., "Transonic Wind Tunnel Tests on an Oscillating Wing with External Stores," AFFDL-TR-78-194, Pts. I-IV, Dec. 1978.

[8]Malone, J.B. and Sankar, L.N., "Numerical Simulation of 2-D Unsteady Transonic Flows Using the Full-Potential Equation," *AIAA Journal*, Vol. 22, Aug. 1984, pp. 1035-1041.

[9]Ballhaus, W.F., and Steger, J.L., "Implicit Approximate Factorization Schemes for the Low-Frequency Transonic Equation," NASA TM X-73082, 1975.

[10]Jameson, A., "Transonic Flow Calculations," *Numerical Methods in Fluid Dynamics*, Hemisphere Publishing Co., Washington, 1978.

[11]Jameson, A. and Caughey, D.A., "A Finite Volume Method for Transonic Potential Flow Calculation," *AIAA Third Computational Fluid Dynamics Conference Proceedings*, 1977, pp. 35-54.

[12]Holst, T.L. and Ballhaus, W.F., "Conservative Implicit Schemes for the Full Potential Equation Applied to Transonic Flows," NASA TM 78469, March 1978.

[13]Goorjian, P.M., "Implicit Computations of Unsteady Transonic Flow Governed by the Full Potential Equation in Conservative Form," AIAA Paper 80-0150, Jan. 1980.

[14]Stone, H.L., "Iterative Solution of Implicit Approximations of Multi-Dimensional Partial Differential Equations," *SIAM Journal of Numerical Analysis*, Vol. 5, No. 3, 1968, pp. 530-550.

[15]Guruswamy, P. and Goorjian, P.M., "An Efficient Coordinate Transformation Technique for Unsteady Transonic Aerodynamic Analysis of Low Aspect Ratio Wings," AIAA Paper 84-0872, Jan. 1984.

[16]Borland, C.J. and Sotomayer, W.A., "An Algorithm for Unsteady Transonic Flow About Tapered Wings," AIAA Paper 84-1567, June 1984.

[17]Malone, J.B. and Sankar, L.N., "Application of a Three-Dimensional Steady and Unsteady Full Potential Method for Transonic Flow Computations," AFWAL-TR-84-3011, May 1984.